Research Square

Preprints are preliminary reports that have not undergone peer review.
They should not be considered conclusive, used to inform clinical practice,
or referenced by the media as validated information.

# A Visual Guided Physics Informed Neural Networks Framework for Real Time Coagulant Dose Optimization in Water Treatment Plants

**Galang Adira Prayoga**
Institut Teknologi Bandung
**Emir Husni**
ehusni@itb.ac.id

Institut Teknologi Bandung
**Reza Darmakusuma**
Institut Teknologi Bandung
**Herto Dwi Ariesyady**
Institut Teknologi Bandung

**Research Article**

**Keywords:** Real-time sensor turbitiy, Physics-informed neural networks (PINNs), Visual information flocculation, Dosage Optimization

**Posted Date:** July 3rd, 2026

**DOI:** https://doi.org/10.21203/rs.3.rs-9755321/v1

**License:** This work is licensed under a Creative Commons Attribution 4.0 International License.
Read Full License

**Additional Declarations:** No competing interests reported.

**Version of Record:** A version of this preprint was published at Discover Artificial Intelligence on October 7th, 2026. See the published version at https://doi.org/10.1007/s44163-026-02372-z.

# A Visual Guided Physics Informed Neural Networks Framework for Real Time Coagulant Dose Optimization in Water Treatment Plants

**Galang Adira Prayoga[1,2], Emir Husni[1], Reza Darmakusuma[1], Herto Dwi Ariesyady[3]**

[1]Departement of Computer Engineering, School of Electrical Engineering and Informatics, Institut Teknologi Bandung, Bandung, 40132 Indonesia
[2]ENTEG-Faculty of Science and Engineering, University of Groningen, Groningen, The Netherlands
[3]Department of Environmental Management Technology, School of Civil and Environmental Engineering, Institut Teknologi Bandung, Bandung, 40132 Indonesia

Corresponding author: Emir Husni (e-mail: ehusni@itb.ac.id).

**ABSTRACT** Real-time sensing and visual information provide significant opportunities to reveal the internal dynamics of flocculation–coagulation processes in water treatment systems. Industrial operations commonly rely on turbidity measurements, while research studies frequently employ the degree of flocculation (DF) as a process indicator. However, both parameters exhibit inherent physical delays because they represent macroscopic outcomes of particle aggregation and sedimentation that require time to become observable. As a result, conventional control strategies depend on reactive adjustments based on previous system states, reducing operational efficiency and limiting prediction accuracy. To overcome these limitations, this study proposes a Real-Time Sensing and Visual Information-Guided Physics-Informed Neural Networks (RTS-VG PINNs) framework. The proposed method integrates real-time sensing, deep visual perception, and governing physical laws into unified learning architecture. A ResNet-50-based feature extractor combined with YOLOv8 is employed to identify regions of interest and extract early-stage predictive features from image sequences. These features are mapped to the time-varying effective sedimentation velocity within the Kynch sedimentation partial differential equation and coupled with the Langmuir–Smoluchowski formulation to estimate optimal coagulant dosage. Experimental results demonstrate that RTS-VG PINNs achieves superior predictive performance compared with purely data-driven models while maintaining low PDE residuals on the order of $10^{-3}$. The framework successfully captures nonlinear relationships among coagulant dosage, turbidity, and zeta potential, reconstructs internal floc density distributions, and provides robust inverse predictions under limited and noisy data conditions.

**INDEX TERMS** Real-time sensor turbitiy; Physics-informed neural networks (PINNs); Visual information flocculation; Dosage Optimization.

## I. INTRODUCTION

Coagulation is an indispensable unit process for reducing turbidity [1] and color in surface water and is employed more than half of the water purification plants [2][3]. As its performance directly affects downstream processes such as flocculation and sand filtration, optimizing coagulation is critical for the overall efficiency of water treatment systems [4]. The effectiveness of coagulation is influenced by multiple factors, including pH [5], temperature [6], electrical conductivity [7], initial turbidity [8], mixing conditions (velocity gradient) [9], and coagulant dosage [10]. In practice, jar tests are commonly used to identify the optimal coagulant dose [11]. However, coagulation involves complex physicochemical interactions that exhibit highly nonlinear behavior [12], making it challenging to develop reliable and generalizable methods for dosage optimization [13].

Real-time sensing and visual observation of the upper liquid layer in thickeners offer a potential approach for inferring the internal dynamics of tailings flocculation–coagulation processes [14][15], as well as for estimating the optimal coagulant dosage . However, conventional turbidity measurements widely used in industry, along with the degree of flocculation (DF) commonly adopted in research [16], suffer from significant response delays relative to the actual flocculation state. This limitation arises because these measurements primarily capture particle concentration and distribution in the supernatant, rather than directly reflecting sedimentation and aggregation

processes occurring deeper within the system [17]. Changes initiated at the bottom of the thickener require time to propagate upward before becoming observable as variations in clarity, leading to a temporal lag in both turbidity and DF measurements [18].

Fundamentally, these indicators represent the cumulative effects of aggregation and settling after they have occurred, rather than providing real-time insight into the evolving behavior of flocs [19]. This mismatch in time scales between measurement and process dynamics restricts traditional control strategies, which rely on delayed feedback and are therefore inherently reactive [20]. As a consequence, operational performance may suffer, including inefficient chemical usage. These challenges are commonly encountered across a wide range of industrial solid–liquid separation systems. Therefore, developing new predictive modeling [21] and control strategies that can overcome measurement lag and capture real process dynamics has important scientific value and urgent industrial demand, becoming a research focus in this field.

Recent studies have increasingly explored the application of machine learning (ML) techniques to optimize coagulant dosage in flocculation–coagulation processes, aiming to overcome the limitations of conventional empirical and jar-test-based approaches. Data-driven models such as Artificial Neural Networks (ANN) [22], Random Forest (RF) [23], Support Vector Machines (SVM) [24], and Gradient Boosting (GB) [25] have been widely reported for predicting optimal coagulant dosage based on water quality parameters, including turbidity, pH, temperature, and organic content. These models have demonstrated strong predictive capabilities and the ability to capture nonlinear relationships inherent in coagulation chemistry. For instance, ANN-based approaches have been successfully used to model coagulant demand under varying influent conditions, while ensemble learning methods such as RF and GB have shown improved robustness against noise and variability in water quality data [13][26]. In addition, recent advances in deep learning have enabled the incorporation of image-based features, where visual information from floc formation is utilized to enhance prediction accuracy and provide additional insight into process dynamics [15][17].

Despite these advancements, purely data-driven approaches remain limited by their dependence on large, high-quality datasets and their lack of physical interpretability [27]. In practical water treatment systems, data are often sparse, noisy, and subject to measurement delays, which can significantly degrade model performance and generalization capability [28]. Moreover, ML models typically learn correlations rather than causation, making them less reliable when operating conditions deviate from the training domain [29]. These limitations have motivated the integration of domain knowledge into learning frameworks.

In this context, Physics-Informed Neural Networks (PINNs) have emerged as a promising paradigm for addressing the challenges of coagulant dosage optimization [29][30][31]. By embedding governing physical laws, such as sedimentation dynamics and particle aggregation kinetics [17], directly into the training process, PINNs provide a principled way to combine data-driven learning with mechanistic understanding. This hybrid approach not only reduces the reliance on large datasets but also improves model interpretability and extrapolation capability under unseen conditions. In flocculation–coagulation systems, PINNs can incorporate models such as the Kynch sedimentation equation [32] and Langmuir–Smoluchowski kinetics to constrain predictions [33][34], enabling more accurate and physically consistent estimation of optimal coagulant dosage. Therefore, PINNs represent a compelling direction for next-generation intelligent control and optimization in water treatment processes.

To address this limitation and potential, this study proposes a novel Real-Time Sensing and Visual Information-Guided Physics-Informed Neural Networks (RTS-VG PINNs) framework, which represents a significant advancement in integrating high-dimensional visual perception with first-principles physical modeling. The key innovation of RTS-VG PINNs lies in its ability to dynamically inform the physics-based model using insights extracted from real-time turbidity measurements and image data. Specifically, deep learning architectures, including ResNet50 and YOLOv8, are employed to capture the evolving characteristics of floc structures from visual observations. These extracted features are subsequently mapped to the time-varying effective sedimentation velocity, $v_0(t)$, which directly modulates the Kynch sedimentation partial differential equation (PDE) embedded within the PINNs framework as a forward (direct) problem.

In parallel, real-time turbidity measurements obtained from sensors at the supernatant layer are utilized to characterize the temporal evolution of suspension clarity. This information is incorporated into the Langmuir–Smoluchowski formulation within the PINNs framework to solve an inverse problem, enabling the estimation of optimal coagulant dosage. By jointly integrating visual and sensor data with governing physical equations, the proposed framework establishes a unified and physically consistent learning architecture.

This study is conducted within a defined set of experimental variables, as illustrated in Fig. 1. The primary independent variable is the coagulant dosage. Key operational parameters include pH, temperature, electrical conductivity, velocity gradient (mixing intensity), initial turbidity, and initial zeta potential, are maintained as control variables throughout the experiments. The system response is evaluated using several dependent variables, namely final turbidity, floc aggregation characteristics (e.g., floc density), and floc settling velocity. Under optimal

conditions, an appropriate coagulant dosage promotes particle destabilization, facilitating effective aggregation and enhancing sedimentation performance.

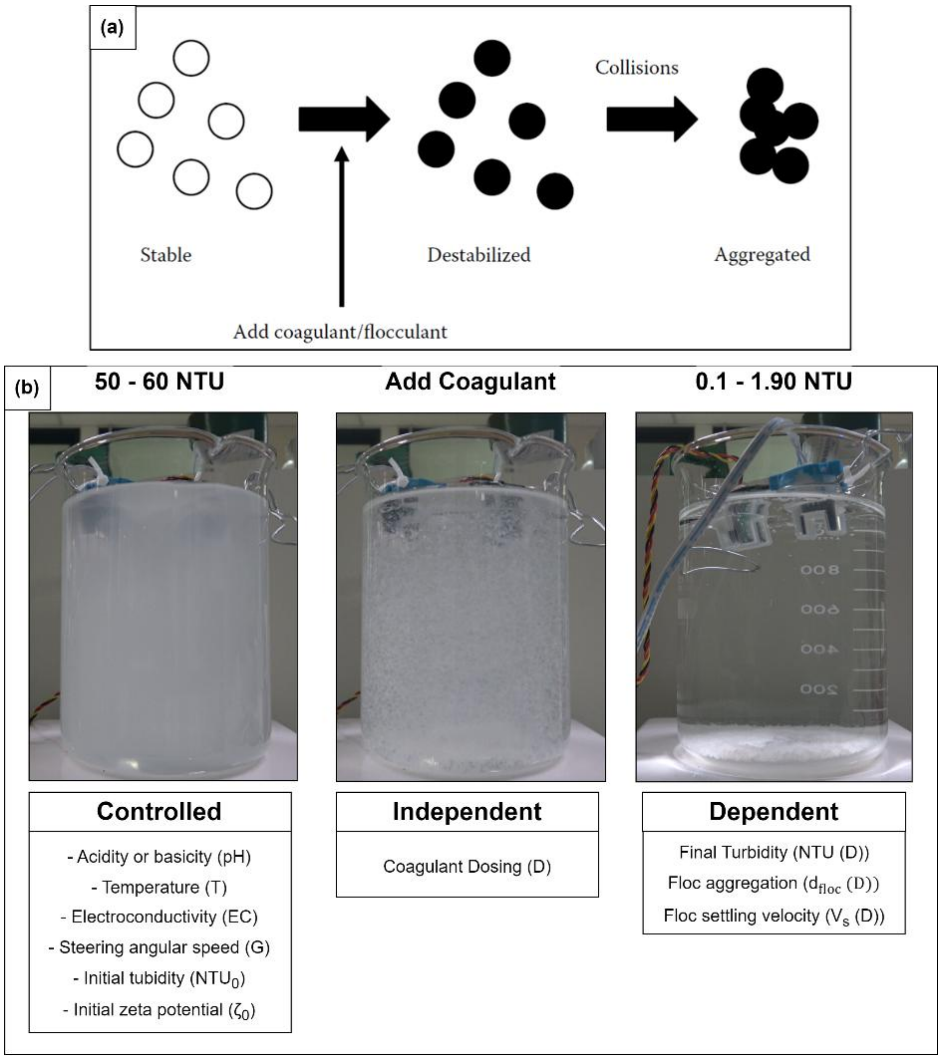



*Figure 1. Variable in experiment (a) coagulant estimation to unstable floc to become aggregated and (b) variables in research*

The performance of RTS-VG PINNs is rigorously evaluated through experimental and comparative analyses. Mechanistic investigations confirm the hypothesized role of visual information in driving the estimation of dynamic sedimentation velocity $v_0(t)$, while turbidity-derived indicators effectively guide coagulant dosage optimization with a physically meaningful time advantage. Furthermore, the framework demonstrates the capability to infer internal concentration fields that are otherwise inaccessible through direct measurement, enabling real-time process understanding and control. Comparative results indicate that RTS-VG PINNs significantly outperforms purely data-driven approaches in predicting optimal coagulant dosage, surpassing conventional machine learning models such as Random Forest (RF), Gradient Boosting (GB), Support Vector Machine (SVM), and Multilayer Perceptron (MLP), particularly under conditions of limited and noisy data.

## II. EXPERIMENTAL MATERIALS AND METHODS

The proposed research adopts a three-stage methodological framework that systematically integrates experimental data acquisition, hybrid physics-informed modeling, and rigorous validation to enable optimal coagulant dosage prediction in flocculation–coagulation processes as shown in Fig.2.

The first stage focuses on constructing a comprehensive dataset that captures both physicochemical and visual dynamics of the coagulation–flocculation process. Experiments are conducted using different types of water samples, including artificial suspensions (e.g., kaolin-based) and natural water sources, to ensure variability and

generalizability. Coagulant dosage is systematically varied across a predefined range to generate diverse process conditions.

During the coagulation–flocculation process, real-time measurements are collected using a water quality monitoring system, which records key parameters such as turbidity, pH, and electrical conductivity. In parallel, visual data are acquired using imaging systems to capture the evolution of floc structures. The process outcomes are quantified through the degree of flocculation (DF), computed using turbidity reduction, image-based analysis (e.g., floc size, morphology, and density) [35], and mass-based measurements. This multimodal dataset is essential for capturing both observable and latent dynamics of the system, forming the foundation for subsequent model development.

The second stage involves the development of a hybrid modeling framework that integrates data-driven learning with physical laws. Visual features extracted from image data using convolutional neural networks (CNNs) [36] are used to infer latent physical variables, particularly the time-varying effective sedimentation velocity $v_0(t)$. This enables the model to incorporate early-stage floc formation dynamics that are not directly measurable through conventional sensors. PINNs is constructed by embedding governing equations, such as mass balance and sedimentation dynamics, into the loss function. These equations act as constraints, ensuring that the model predictions remain physically consistent. The integration of these components results in RTS-VG PINNs model, where visual information dynamically informs the physical parameters, and real-time sensor data guide the inverse estimation of optimal coagulant dosage. This dual coupling enables the model to bridge observable data with underlying process mechanisms.

In the final stage, the proposed RTS-VG PINNs framework is rigorously evaluated using cross-validation techniques and quantitative error metrics. The model's predictive performance is assessed in terms of its ability to accurately estimate key process variables, including degree of flocculation and optimal coagulant dosage.

### A. Experimental system and data foundation

The experimental setup was designed to enable synchronized acquisition of physicochemical measurements and visual data during the flocculation–coagulation process, as illustrated in Fig. 3. Water samples were prepared using both natural and artificial sources to ensure variability in initial conditions. The natural water samples consisted of PDAM water with turbidity in the range of 50–60 NTU, while artificial samples were prepared using tap water and aquades, both with and without kaolin addition (50 mg/L) to simulate controlled turbidity conditions. The physicochemical characteristics of the samples varied within representative ranges, with pH values approximately between 6.2 and 7.8, electrical conductivity (EC) ranging from low-conductivity aquades (≈1–6 μS/cm) to higher-conductivity tap and PDAM water (≈150–250 μS/cm), and initial zeta potential values between −3.1 mV and 0.3 mV. These variations reflect realistic water treatment conditions and provide a diverse dataset for model training and validation.

Coagulant dosing was systematically applied using polyaluminum chloride (PAC) [37], with dosages defined in the range of 12–120 mg/L. The corresponding liquid volume of coagulant ($V_{mL}$) was determined based on a conversion relationship that accounts for coagulant density, sample volume, and dilution factor:

$$V_{mL} = \frac{D \times V_s}{\rho \times 1000 \div DF} \tag{1}$$

where $\rho = 1.2$ g/mL is the coagulant density, $V_s = 1$ L is the sample volume, and $DF = 100$ is the dilution factor. Based on this formulation, the applied dosing range corresponds to approximately 1–10 mL of diluted coagulant solution, with 2–7 mL (24–84 mg/L) identified as the working operational range for effective flocculation based on visual flocculation.

Real-time water quality parameters, including turbidity, pH, and electrical conductivity, were measured using a calibrated water quality meter and turbidity sensor. In parallel, a custom-built sensing module equipped with embedded electronics was deployed to continuously monitor turbidity dynamics at the supernatant layer. To capture the evolution of floc structures, a high-resolution camera system was positioned in front of the reactor, supported by controlled lighting to ensure consistent image quality and minimize noise. The camera recorded time-series images throughout the process, enabling extraction of floc size, morphology, and spatial distribution.

All sensor readings and visual data were synchronized and logged through a central computing system for further processing. Prior to model development, the collected data were preprocessed, including noise filtering, normalization, and temporal alignment between sensor signals and image sequences. This integrated data acquisition

framework ensures that both observable measurements and latent visual features are consistently captured, providing a high-quality dataset for training and validating the proposed RTS-VG PINNs model.

.

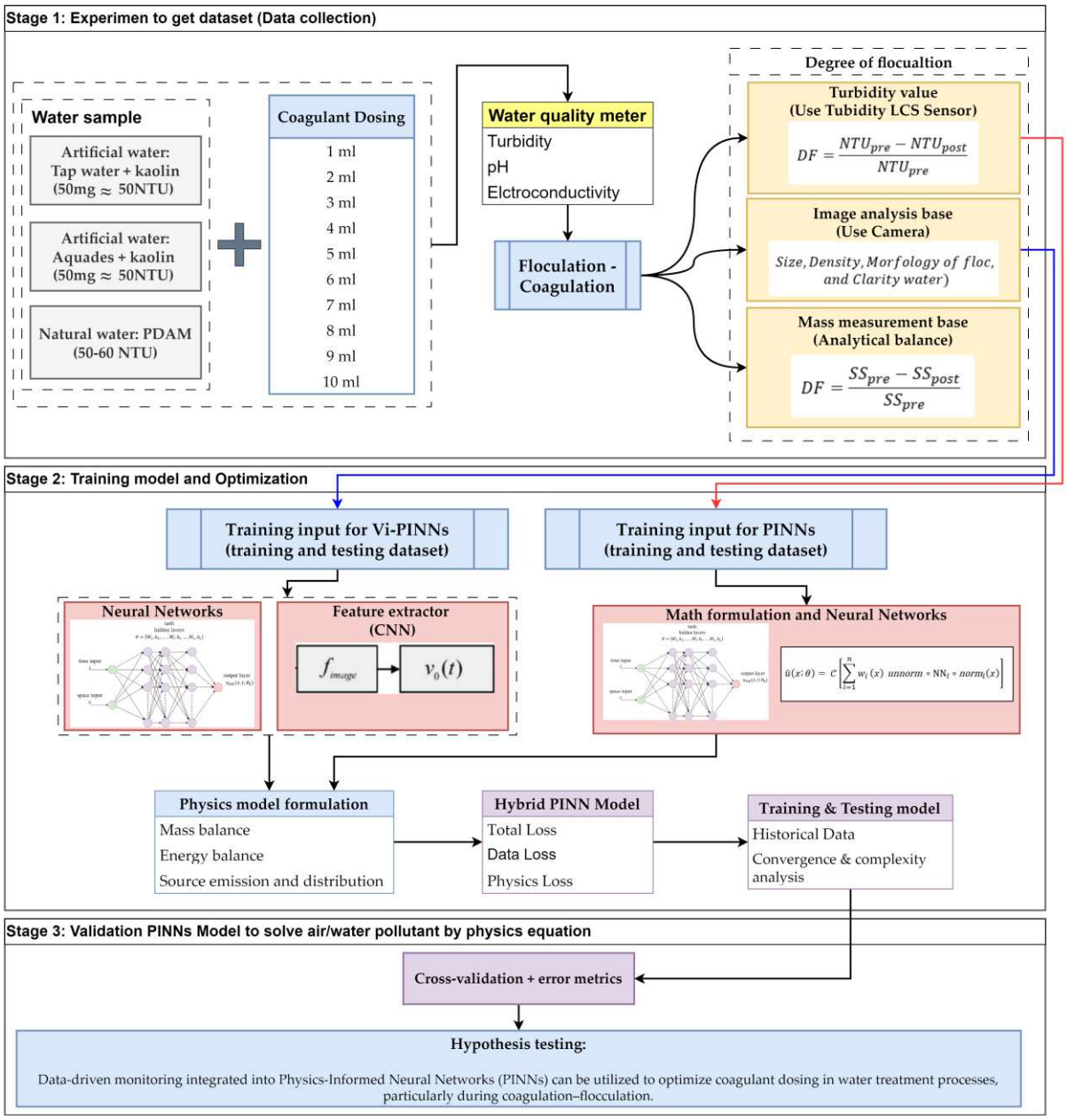



*Figure 2. Desain methodology research*

## B. Visual Guided-Enhanced Physics-Informed neural network (VG-PINNs) architecture and information flow

Image data were collected using a controlled visual acquisition system to capture the temporal evolution of flocculation dynamics during the coagulation–flocculation process as shown in Fig.4. A Canon 250D camera was employed to record high-resolution video at 60 frames per second with a resolution of 1920×1080 pixels, ensuring sufficient spatial and temporal detail for feature extraction. The recording protocol was designed to cover the complete process, including rapid mixing at 200 rpm for 2 minutes, followed by slow mixing at 30 rpm for 10 minutes, and a subsequent settling phase of 5 minutes. The camera was positioned in front of the jar test to provide a clear and consistent field of view, while lighting conditions were controlled to minimize reflection and ensure image quality.

From the recorded video sequences, frames were extracted and preprocessed to generate image datasets for training CNN. Regions of interest (ROI) were defined within the observation window to focus on representative floc

behavior while reducing background noise. This approach enables the CNN model to learn meaningful visual features related to floc size, morphology, and spatial distribution, which are critical for inferring underlying process dynamics and supporting the estimation of sedimentation-related parameters within the proposed RTS-VG PINNs framework.




*Figure 3. Data preparation and setup device to collect data experimental*

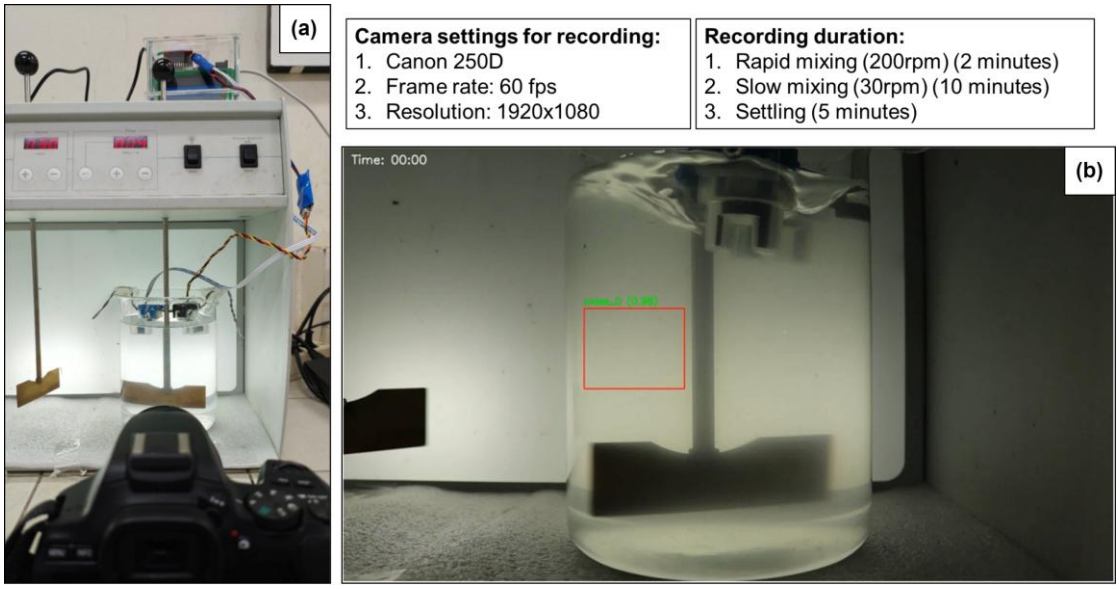



*Figure 4. Image data collecting to train CNN model*

The proposed framework employs two complementary CNN architectures to capture floc dynamics with both high sensitivity and real-time capability. As illustrated in Fig. 5(a), a two-stage detection approach based on ResNet-50 [38] is adopted to enable high-resolution feature extraction. The architecture begins with an initial convolutional layer followed by four residual block stages with increasing depth, allowing hierarchical learning of low-level textures to high-level semantic representations of floc structures. The use of residual connections mitigates gradient degradation and facilitates deeper network training, thereby enhancing sensitivity to subtle

variations in floc morphology, density, and distribution. The extracted features are then aggregated through global average pooling and passed through fully connected layers to produce regression or classification outputs related to floc characteristics, such as degree of flocculation (DF).

In parallel, as shown in Fig. 5(b), a one-stage detection framework based on YOLOv8 [39][40] is implemented to support real-time detection and tracking of floc evolution. Unlike the two-stage approach, YOLOv8 performs feature extraction and object detection in a unified architecture, significantly reducing computational latency. The model consists of sequential convolutional blocks and cross-stage feature fusion modules, enabling efficient multi-scale feature representation. This structure allows the model to rapidly identify and localize floc regions while maintaining competitive accuracy. The final classification head outputs floc-related features or DF estimates, which are subsequently integrated into the RTS-VG PINNs framework.

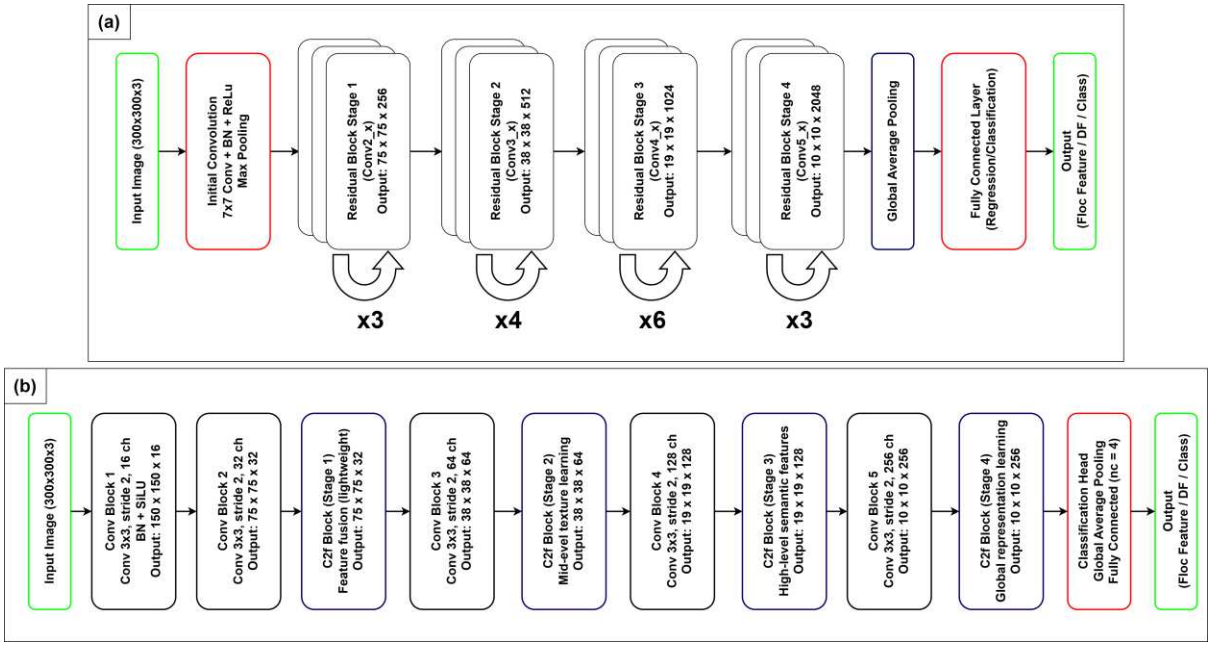



*Figure 5. CNN model architecture of (a) two stage detection use resnet-50 for high sensitivity detection and (b) one stage detection uses Yolov8 for real time detection*

The dataset was systematically constructed to capture the temporal evolution and dosage-dependent behavior of the flocculation–coagulation process. As illustrated in Fig. 6, experiments were initially conducted across a wide range of coagulant dosages (1–10 mL, equivalent to 12–120 mg/L) to cover diverse operating conditions. However, based on experimental observations, the most representative and effective flocculation behavior was identified within the range of 2–7 mL (12–84 mg/L), and this subset was selected for dataset construction and model training.

Within this selected range, image samples were categorized into four distinct stages of floc evolution according to reaction time: early dispersion (0–1 min, Class 0), initial aggregation (3–4 min, Class 1), floc growth and densification (11–12 min, Class 2), and settling/clarification phase (16–17 min, Class 3). Each class reflects characteristic physicochemical transitions, from dispersed colloidal particles to the formation of dense flocs and subsequent sedimentation.

The dataset integrates both visual observations and conceptual understanding of the flocculation mechanism, where coagulant species interact with suspended particles (e.g., organic matter and colloids) to promote aggregation. Image regions of interest (ROI) were extracted to ensure consistency and reduce background interference, allowing the CNN model to focus on relevant features such as floc size, morphology, and spatial distribution. By organizing the dataset across both temporal stages and optimal dosage conditions, the model is trained to capture the dynamic evolution of floc formation as well as its sensitivity to coagulant dosage. This structured dataset provides a robust foundation for supervised learning and supports accurate feature extraction for subsequent integration within the RTS-VG PINNs framework.

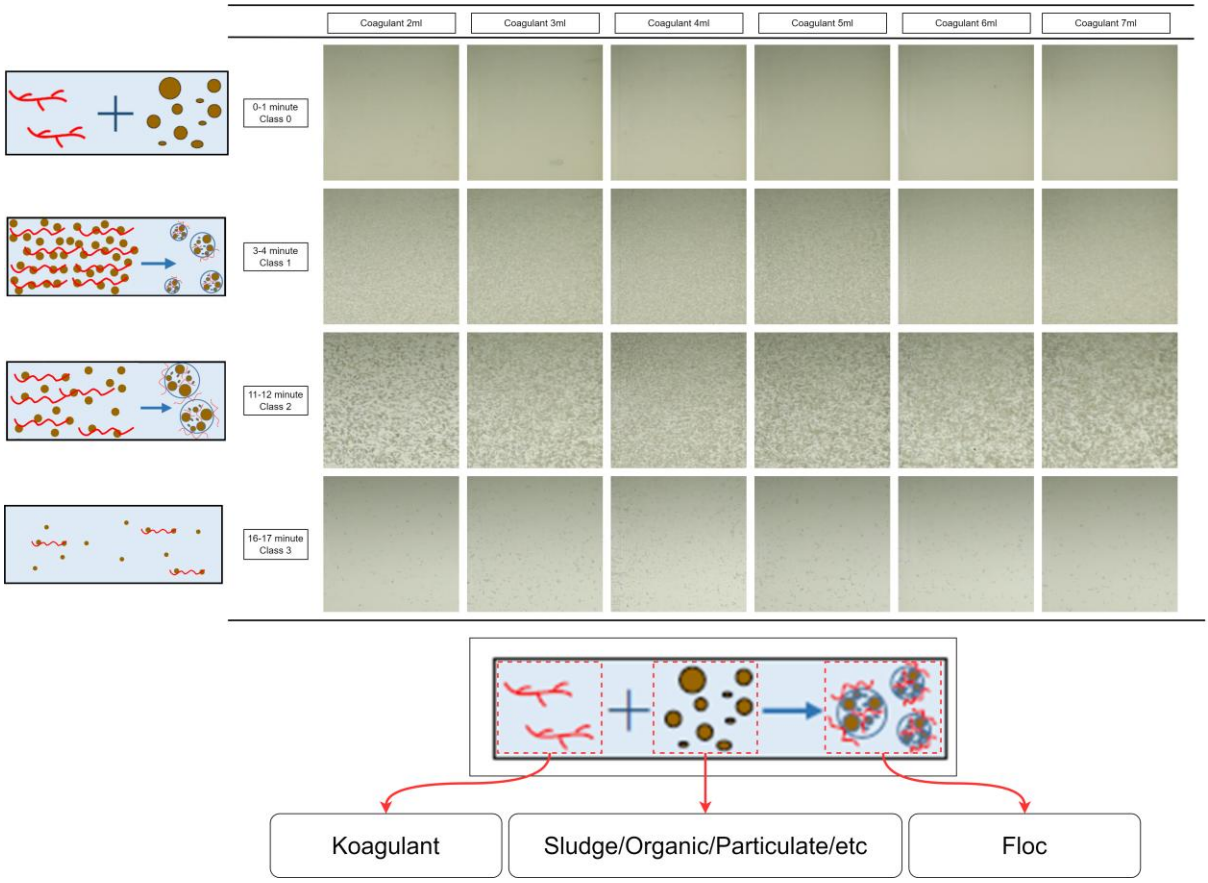



*Figure 6. Dataset of flocculation to train CNN model*

### C. Physical model and Data-Driven parameters

The proposed PINNs framework models the flocculation–settling process as a direct solution of the governing Kynch sedimentation equation, enabling the estimation of the spatiotemporal floc density distribution $\phi(t,z)$ shown in Fig. 7. The neural network, parameterized by trainable weights $\theta$, takes time and spatial coordinates as inputs, $x=(t,z)$, and outputs the floc concentration field $y=\phi_{pred}=\phi_{NN}(t,z;\theta)$. A key aspect of this framework is that the training data are not solely obtained from direct measurements but are partially inferred from CNN applied to image data. Specifically, visual features extracted using CNN models (e.g., ResNet-50 and YOLOv8) are used to estimate the time-varying sedimentation velocity $v_0(t)$ that obtain from CNN feature $g(f_{image}(t))$, while also providing indirect information related to floc structure and degree of flocculation (DF). These CNN-derived features act as an intermediate bridge between raw visual observations and the physics-based model.

The learning process is governed by a composite loss function that integrates physical constraints and observational consistency, defined as:

$$\mathcal{L}_{Total}=\mathcal{L}_{phy}(\theta)+\mathcal{L}_{data}(\theta)+\mathcal{L}_{IC}(\theta)+\mathcal{L}_{BC}(\theta) \tag{2}$$

where $\lambda_{phy},\lambda_{data},\lambda_{IC},\lambda_{BC}$ are weighting coefficients that balance each component. The physics loss ($\mathcal{L}_{phy}$) enforces the Kynch sedimentation equation by minimizing the residual of the governing partial differential equation:

$$L_{phy}=\frac{\lambda_{phy}}{N_{phy}}\sum_{i=1}^{N_{phy}}\left|\frac{\partial\phi_{pred}}{\partial t}+\frac{\partial F\left(\phi_{pred},t\right)}{\partial z}\right|^{2}_{(t_i,z_i)} \tag{3}$$

ensuring that the predicted solution satisfies mass conservation and sedimentation dynamics. The data loss ($\mathcal{L}_{data}$) incorporates experimental observations through:

$$\mathcal{L}_{data} = \frac{\lambda_{data}}{N_{data}} \sum_{i=1}^{N_{data}} \left|\phi_{pred} - \phi_{data}(t_i)\right|^2 \tag{4}$$

which constrains the model at the observation boundary. The initial condition loss ($\mathcal{L}_{IC}$) is defined as:

$$\mathcal{L}_{IC} = \frac{\lambda_{IC}}{N_{ic}} \sum_{i=1}^{N_{ic}} \|\phi(0, z_i) - \phi_0(z_i)\|^2 \tag{5}$$

while the boundary condition loss ($\mathcal{L}_{BC}$) enforces a no-flux constraint at the top surface:

$$L_{BC} = \frac{\lambda_{BC}}{N_{bc}} \sum_{i=1}^{N_{bc}} \left\| \frac{\partial \phi_{pred}}{\partial z} \left( v_0(t)(1 - \phi_{pred})^n \right) \right\|^2 \tag{6}$$

Through this multi-objective optimization, the PINNs framework simultaneously learns from data while adhering to first-principles physics, enabling robust reconstruction of internal floc density fields that are otherwise inaccessible to direct measurement. The incorporation of the time-varying sedimentation velocity $v_0(t)$, inferred from visual feature extraction, further enhances the model's ability to adapt to evolving floc characteristics. This formulation provides a physically consistent and data-efficient approach for modeling flocculation dynamics.

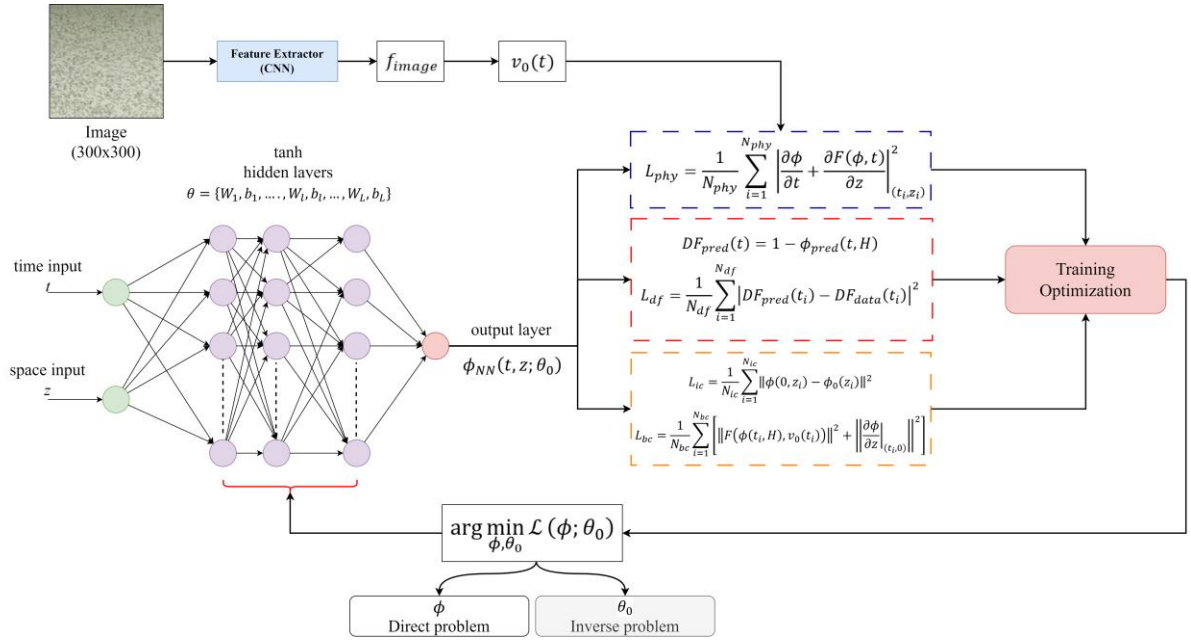



*Figure 7. Direct solution of flocculation process to approximate floc density distribution*

Fig. 8 presents the inverse modeling framework, where PINNs is employed to approximate the optimal coagulant dosage by learning the underlying physicochemical relationships governing flocculation–coagulation processes. In this formulation, the model takes as input a set of initial operational and water quality variables, $\mathbf{x} = \{pH, T, G, \zeta_0, NTU_0\}$, where $pH$ is acidity, $T$ is temperature, $G$ is the velocity gradient, $\zeta_0$ is the initial zeta potential, and $NTU_0$ is the initial turbidity.

The network outputs multiple process-related variables, $\mathbf{y} = \{\zeta(D), NTU(D), d_{floc}(D), v_s(D)\}$, representing the evolution of zeta potential, turbidity, floc size, and settling velocity as functions of dosage (D). Unlike the direct problem, this inverse formulation aims to infer the optimal dosage condition by learning how system states evolve with respect to $D$.

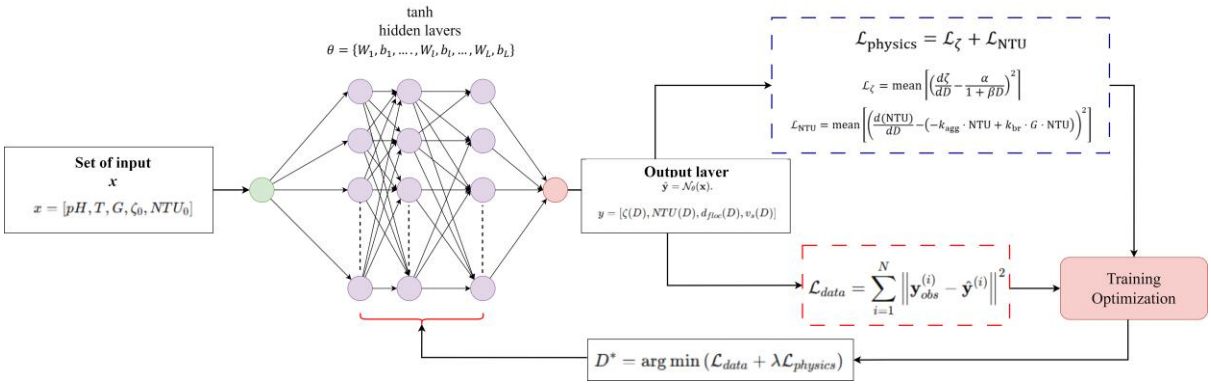



*Figure 8. Invers solution of flocculation process to approximate optimal dosing of coagulant*

To ensure physical consistency, the learning process incorporates governing equations derived from Langmuir-type adsorption kinetics and the Smoluchowski coagulation framework. The variation of zeta potential with dosage is constrained by:

$$\frac{d\zeta}{dD} = \frac{\alpha}{1+\beta D} \tag{7}$$

which captures the nonlinear adsorption behavior characterized by an initial rapid response followed by saturation. In parallel, turbidity evolution is modeled through the aggregation–breakup balance:

$$\frac{d(NTU)}{dD} = -k_{agg} \cdot NTU + k_{br} \cdot G \cdot NTU \tag{8}$$

where $k_{agg}$ and $k_{br}$ denote learning able aggregation and breakup rate constants, respectively. These physical relationships are embedded into the PINNs framework through mean squared error (MSE)-based residual losses:

$$\mathcal{L}_\zeta = \frac{\lambda_\zeta}{N_\zeta} \sum_{i=1}^{N_\zeta} \left[ \left( \frac{d\zeta(D)}{dD} - \frac{\alpha}{1+\beta D} \right)^2 \right] \tag{9}$$

$$\mathcal{L}_{NTU} = \frac{\lambda_{phy}}{N_{phy}} \sum_{i=1}^{N_{phy}} \left[ \begin{pmatrix} \frac{d(NTU(D))}{dD} \\ +k_{agg} \cdot NTU(D) \\ -k_{br} \cdot G \cdot NTU(D) \end{pmatrix}^2 \right] \tag{10}$$

The total training objective combines data fidelity and physical constraints:

$$\mathcal{L}_{data} = \frac{\lambda_{data}}{N_{data}} \sum_{i=1}^{N_{data}} \left| y_{data}(t_i) - y_{pred}(t_i, x) \right|^2 \tag{11}$$

$$\mathcal{L}_{physics} = \mathcal{L}_\zeta + \mathcal{L}_{NTU} \tag{12}$$

$$\mathcal{L}_{total} = \mathcal{L}_{data} + \mathcal{L}_{physics} \tag{13}$$

where $\mathcal{L}_{data}$ measures the discrepancy between predicted and observed values, and $\mathcal{L}_{phy}$ balances the contribution of physics-based regularization. Through this formulation, the model is guided to satisfy both adsorption-driven surface charge dynamics and aggregation–breakup mechanisms governing turbidity evolution.

By jointly learning these relationships, the inverse PINNs framework is able to identify the optimal coagulant dosage corresponding to the equilibrium condition where aggregation and breakup are balanced. This approach not only improves prediction accuracy under limited or noisy data but also ensures that the inferred solutions

remain physically interpretable. Consequently, the proposed method provides a robust and principled tool for real-time coagulant dosage optimization in flocculation–coagulation systems.

### D. Training Details

The model was trained using 10 independent experimental datasets, each comprising synchronized $DF(t)$time series and corresponding image sequences. The dataset was partitioned into training and validation subsets with an 80:20 split based on experimental batches to preserve temporal and process consistency. To ensure adequate coverage of the solution space, Latin hypercube sampling was employed to generate collocation points, including 2,000 physics points, 50 data points, 200 boundary condition points, and 200 initial condition points. The training process was conducted using the AdamW optimizer with an initial learning rate of $1 \times 10^{-3}$, which was reduced by 50% every 5,000 iterations over a total of 20,000 training steps [41].

### E. Performance evaluation methods and benchmarks

The physical consistency of the proposed VI-PINNs model was evaluated by examining the convergence behavior of the physics-based loss term and analyzing the spatial distribution of partial differential equation (PDE) residuals across the solution domain, ensuring adherence to the governing physical laws. To further validate the internal mechanisms and enhance interpretability, the temporal evolution of the predicted sedimentation velocity $v_0(t)$ was analyzed in relation to the auxiliary visual indicator $V_{\text{contrast}}(t)$, providing insight into how visual features inform the physical model. Additionally, the plausibility of the inferred internal concentration field $\phi(t, z)$ was assessed to confirm that the direct solution produces physically meaningful representations of floc distribution and settling dynamics.

For the inverse solution, the predictive performance of the RTS-VG PINNs framework was benchmarked against several conventional machine learning models, including Random Forest (RF), Gradient Boosting (GB), Support Vector Machine (SVM), and Multilayer Perceptron (MLP). Model performance was quantitatively evaluated using standard regression metrics, including the coefficient of determination ($R^2$), root mean square error (RMSE), and mean absolute error (MAE). These metrics provide complementary perspectives on model accuracy, capturing goodness-of-fit, sensitivity to large errors, and overall prediction deviation. Comparative analysis enables a comprehensive assessment of the robustness and generalization capability of the proposed framework, particularly under conditions of limited and noisy data.

## III. EXPERIMENTAL RESULTS AND ANALYSIS

### A. Analysis degree of flocculation

Fig. 9 presents the temporal evolution of turbidity and the corresponding degree of flocculation (DF) under varying coagulant dosages, obtained from real-time turbidity sensor measurements. As shown in Fig. 9(a), turbidity exhibits distinct dynamic behavior depending on the applied dosage. At lower dosages (e.g., 1–3 mL), turbidity reduction is relatively slow and incomplete, indicating insufficient particle destabilization and weak aggregation. In contrast, moderate dosages (approximately 4–7 mL) demonstrate a more pronounced and rapid decline in turbidity, particularly after the transition from slow mixing to the settling phase (around 10–12 minutes), suggesting effective floc formation and sedimentation. For higher dosages, the improvement becomes marginal or less stable, which may indicate overdosing effects such as charge reversal or restabilization of particles.

The corresponding degree of flocculation, shown in Fig. 9(b), further highlights these trends. During the early stage (0–5 minutes), DF values remain relatively low or even negative, reflecting the dominance of mixing and initial particle interactions. As the process progresses, DF increases significantly for optimal dosage ranges, reaching peak values during the settling phase. Notably, coagulant dosages in the range of 2–7 mL yield the most consistent and stable increase in DF, confirming this interval as the effective operating window for flocculation. Beyond this range, DF improvement plateaus or exhibits fluctuations, indicating diminishing returns in aggregation efficiency.

These observations demonstrate that real-time turbidity measurements provide a reliable proxy for quantifying flocculation dynamics and identifying optimal dosing conditions. The time-dependent behavior of DF also reveals a clear lag between initial mixing and observable clarification, emphasizing the importance of predictive modeling to anticipate process evolution. This experimental analysis forms the basis for subsequent model validation, where the RTS-VG PINNs framework leverages both temporal turbidity data and visual information to enhance prediction accuracy and enable proactive coagulant dosage optimization.

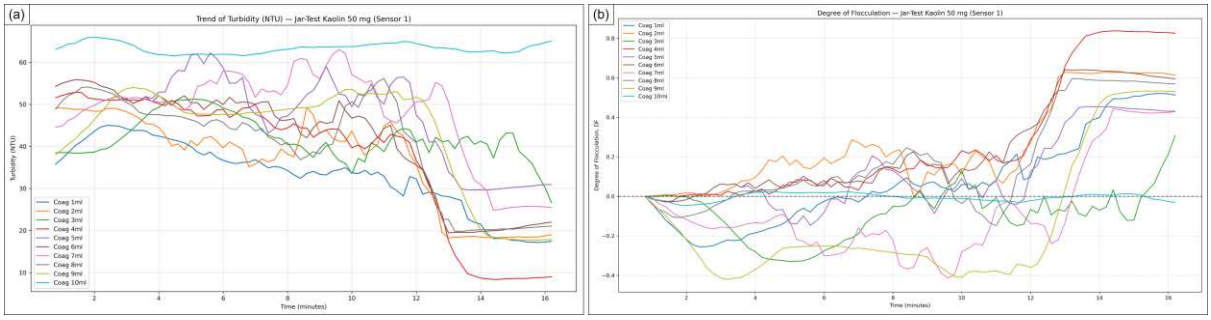



*Figure 9. Turbidity changes over time and degree of flocculation based on coagulant dosing*

## B. Settling rate driven by visual information

Fig.10 illustrates the performance of CNN models in classifying the evolution of floc density, which serves as a visual proxy for inferring sedimentation dynamics. The results are presented for two complementary architectures: ResNet50 (two-stage feature extractor) and YOLOv8 (one-stage real-time detector).

The training and validation performance of the ResNet50 model are shown in Fig. 10(a) and Fig. 10(b). The loss curve in Fig. 10(a) demonstrates a consistent decrease over epochs, while the accuracy curve in Fig. 10(b) shows rapid improvement followed by stabilization at a high level. The relatively small gap between training and validation accuracy indicates good generalization capability, suggesting that ResNet50 effectively learns discriminative features related to floc density and structure.

In contrast, the performance of the YOLOv8 model is presented in Fig. 10(c)–(e). As shown in Fig. 10(c), the training loss decreases steadily, indicating stable optimization behavior. The accuracy trend in Fig. 10(d) reveals that the model quickly converges and maintains consistent performance, demonstrating its suitability for real-time applications. The normalized confusion matrix in Fig. 10(e) further confirms the model's classification capability, with high accuracy observed along the diagonal (e.g., above 0.90 for most classes). Misclassifications are primarily limited to neighboring classes, reflecting the gradual transition between flocculation stages rather than model instability.

The combination of these two models provides complementary strengths. ResNet50 offers high sensitivity and robust feature extraction for capturing subtle variations in floc morphology, while YOLOv8 enables efficient real-time detection and classification. Importantly, the visual features extracted from both models are subsequently mapped to the time-varying sedimentation velocity $v_0(t)$, enabling the integration of visual information into the physics-based PINNs framework. As floc density increases, these models capture the structural evolution of flocs and translate it into physically meaningful settling behavior.

The results demonstrate that visual information serves as a leading indicator of sedimentation dynamics, allowing earlier detection of floc development compared to turbidity-based measurements. This capability plays a crucial role in reducing measurement lag and enhancing the predictive performance of the proposed RTS-VG PINNs framework.

Fig. 11 illustrates the ability of the vision-based model to quantify and track floc density evolution throughout the entire coagulation–flocculation process using confidence-level detection. As shown in Fig. 11(a), the CNN model assigns confidence scores to different floc density classes, effectively distinguishing between stages of dispersion, aggregation, densification, and settling. These confidence values reflect the model's certainty in identifying the structural characteristics of flocs, such as size, compactness, and spatial distribution, across varying process conditions.

Fig. 11(b) presents the temporal mapping of floc density based on the detected confidence levels over the full operational sequence, including rapid mixing (2 minutes), slow mixing (10 minutes), and settling (5 minutes). The raw and smoothed signals of the flocculation indicator demonstrate a clear progression through distinct classes, corresponding to different physical regimes of the process. During the rapid mixing phase, the confidence values remain relatively stable, indicating a predominantly dispersed state. As the system transitions into slow mixing, fluctuations in confidence reflect active particle collisions and the formation of initial aggregates. In the later stages, the confidence level increases and stabilizes, corresponding to the development of dense flocs and the onset of sedimentation.

A key observation from Fig. 11(b) is the identification of the interface arrival time ($t_s$), marked by a sharp transition in the confidence signal. This point signifies the moment when floc settling becomes dominant and the clarification front reaches the observation region. The ability to detect this transition from visual data provides a

critical advantage over traditional turbidity-based measurements, which typically exhibit delayed responses. By mapping floc density evolution in real time, the model offers a more responsive and physically meaningful representation of process dynamics.

These results demonstrate that confidence-based visual detection serves as an effective proxy for monitoring flocculation stages and identifying key transition points within the process. This capability plays a crucial role in informing the estimation of sedimentation velocity $v_0(t)$ and enhances the integration of visual information within the RTS-VG PINNs framework for improved prediction and control of coagulant dosing

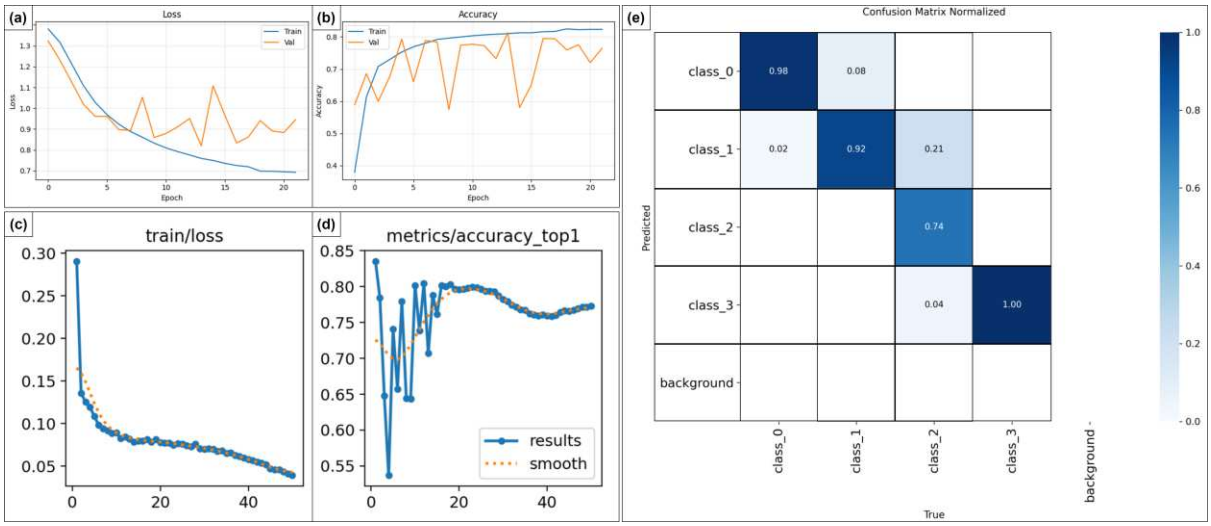



*Figure 10. Performance CNN model to classify the changing density floc*

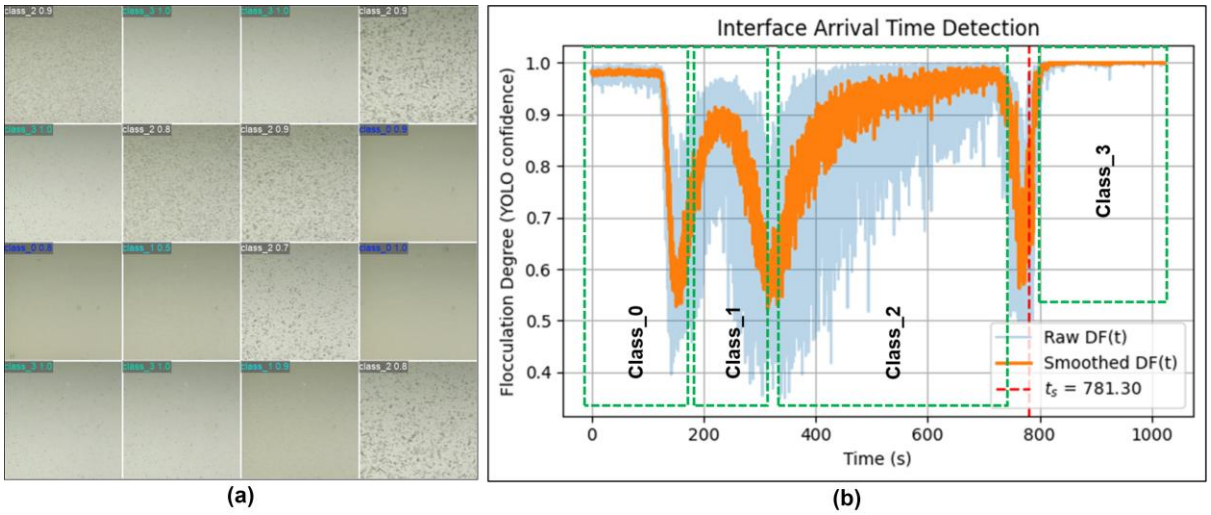



*Figure 11. (a) Confidence level detection of floc density and (b) mapping the floc density based on confidence level detection in whole proses coagulation-flocculation (two-minute rapid mixing, ten-minute slow mixing, and five-minute settling)*

Fig. 12 presents the transformation of visually inferred floc density, obtained from CNN-based confidence levels, into a physically meaningful floc density distribution suitable for integration within the PINNs framework. As shown in Fig. 12(a), the degree of flocculation $DF(t)$ is first derived from the confidence scores associated with each flocculation class. These classes represent distinct physical stages of the process, ranging from dispersed particles (Class 0) to fully developed and settling flocs (Class 3). To quantify this relationship, a weighted mapping

is employed, where the confidence level of each class is multiplied by a corresponding normalized turbidity degree. Specifically, the conversion is defined as:

$$DF(t) = \text{Confidence}_{class_n}(t) \times \text{NTU_degree}_{class_n} \tag{14}$$

where the assigned NTU degree reflects the relative clarity or turbidity associated with each flocculation stage (e.g., 0.1, 0.3, 0.8, and 1.0 for Classes 0–3, respectively). This formulation enables the conversion of qualitative visual classifications into a continuous quantitative indicator of flocculation dynamics.

To reduce noise and enhance temporal consistency, the raw $DF(t)$ signal is further smoothed, as illustrated in Fig. 12(a). The resulting smoothed DF curve captures the progressive evolution of floc formation, including the transition from initial dispersion to aggregation and eventual settling. Subsequently, this DF signal is mapped into the solid volume fraction $\phi(t)$, as shown in Fig. 12(b), using the relationship between turbidity reduction and particle concentration. The mapped $\phi(t)$ exhibits a decreasing trend over time, reflecting the removal of suspended particles due to floc aggregation and sedimentation, with a sharp decline observed during the settling phase.

This conversion process plays a critical role in bridging visual information and physical modeling. By transforming CNN-derived confidence levels into a physically interpretable concentration field, the approach enables seamless integration of image-based observations into the PINNs framework. As a result, the model is able to leverage visual data not only for classification but also for reconstructing internal system states, thereby enhancing the accuracy and responsiveness of flocculation process modeling and control.

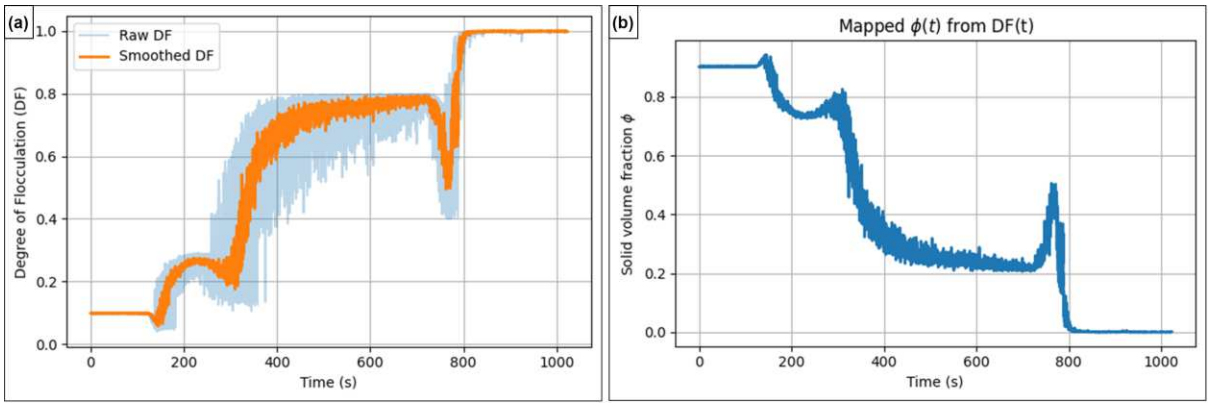



*Figure 12. Result of conversion from density floc measured by confidence level to density distribution*

### C. VG-PINNs prediction capability for internal spatiotemporal concentration field ϕ (t, z)

Fig. 13 presents the performance of the direct solution PINNs solution in reconstructing the floc density distribution during the flocculation–coagulation process. The results demonstrate the ability of the model to achieve both numerical convergence and physical consistency while accurately capturing the underlying process dynamics.

The training behavior of the model is illustrated through the evolution of loss components, where the total loss, physics loss (PDE residual), data loss, and initial condition loss all exhibit stable convergence over training iterations. Notably, the physics loss decreases to a very low magnitude, indicating that the predicted solution closely satisfies the governing Kynch sedimentation equation. This confirms that the model is not only fitting the data but also adhering to the underlying physical laws, which is a key advantage of the PINNs framework.

The predictive accuracy at the observation boundary ($z = H$) is shown by comparing the PINNs output with experimental data. The model demonstrates strong agreement with the observed volume fraction derived from the degree of flocculation, successfully capturing key dynamic features such as the gradual decrease in particle concentration, transitional fluctuations during aggregation, and the sharp drop associated with the onset of settling. Minor deviations are observed during rapid transitions, which can be attributed to measurement noise and the inherent complexity of flocculation dynamics.

Furthermore, the reconstructed spatiotemporal floc density field $\phi(t, z)$ provides valuable insight into the internal behavior of the system. The predicted field shows a clear stratification pattern, with higher particle

concentrations at lower depths and progressively lower concentrations toward the top, consistent with physical expectations of sedimentation. The movement of the interface over time is also captured, reflecting the downward progression of flocs and the clarification of the supernatant layer.

These results demonstrate that the proposed direct PINNs solution is capable of accurately reconstructing the internal floc density distribution while maintaining strong physical consistency. This capability is particularly significant, as such internal states are typically inaccessible through direct measurement. The integration of physics constraints with CNN-informed inputs enables a robust and interpretable modeling framework, forming a solid foundation for subsequent inverse analysis and real-time coagulant dosage optimization.

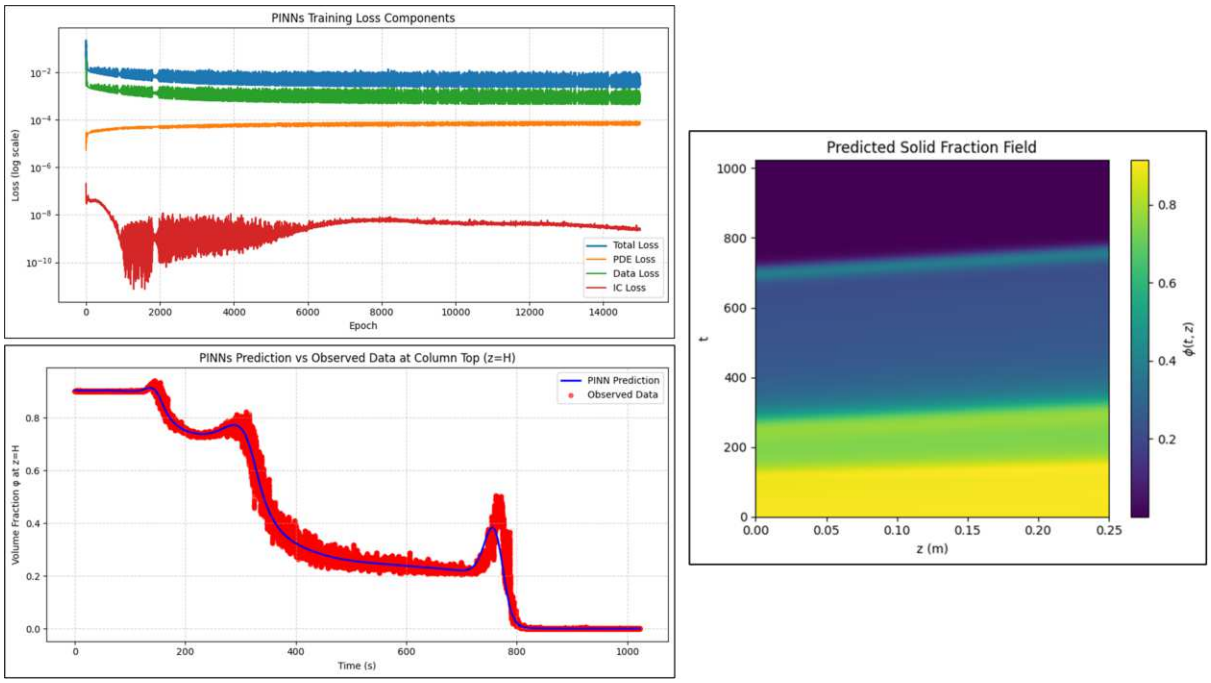



*Figure 13. Performa of direct solution to approximation floc density distribution in flocculation-coagulation process*

## D. Performance evaluation of VG-PINNs in approximate optimal dosing

Fig. 14 presents the performance of the inverse solution PINNs in estimating the optimal coagulant dosage for the flocculation–coagulation process. The results demonstrate the capability of the proposed framework to achieve stable convergence while capturing the underlying physicochemical mechanisms governing dosage optimization.

The training dynamics without uncertainty regularization are shown in Fig. 14(a), where the total loss and its components, including data loss, physics loss, charge neutralization loss (zeta potential), and aggregation loss (turbidity evolution), exhibit a consistent decreasing trend. This indicates stable optimization and effective learning of both data-driven and physics-based relationships. Correspondingly, Fig. 14(b) shows that the predicted optimal dosage rapidly converges after an initial transient phase and stabilizes within a narrow range, demonstrating strong convergence behavior and reliability of the inverse formulation.

In contrast, Fig. 14(c) and Fig. 14(d) present the training results when Monte Carlo dropout is incorporated into the model. The loss curves in Fig. 14(c) show a more fluctuating pattern compared to the deterministic case, reflecting the stochastic nature of dropout during training. However, the overall downward trend confirms that the model still converges while benefiting from improved regularization. The corresponding optimal dosage evolution in Fig. 14(d) exhibits higher variability, capturing a distribution of possible solutions rather than a single deterministic estimate. This behavior reflects the model's ability to account for uncertainty arising from noisy data and complex system dynamics.

Importantly, despite the increased variability, the predicted dosage values remain within a physically consistent range, aligning with the experimentally observed optimal dosing window. The inclusion of Monte Carlo dropout enhances the robustness of the inverse PINNs framework by preventing overfitting and enabling uncertainty-aware predictions. This is particularly valuable in real-world water treatment systems, where measurements are often noisy and operating conditions are subject to variability.

The results demonstrate that the inverse PINNs framework can reliably estimate optimal coagulant dosage under both deterministic and stochastic training settings. While the deterministic model provides stable point estimates, the Monte Carlo dropout-enhanced model offers additional insight into prediction uncertainty, making it a more robust and practical solution for real-time process optimization.

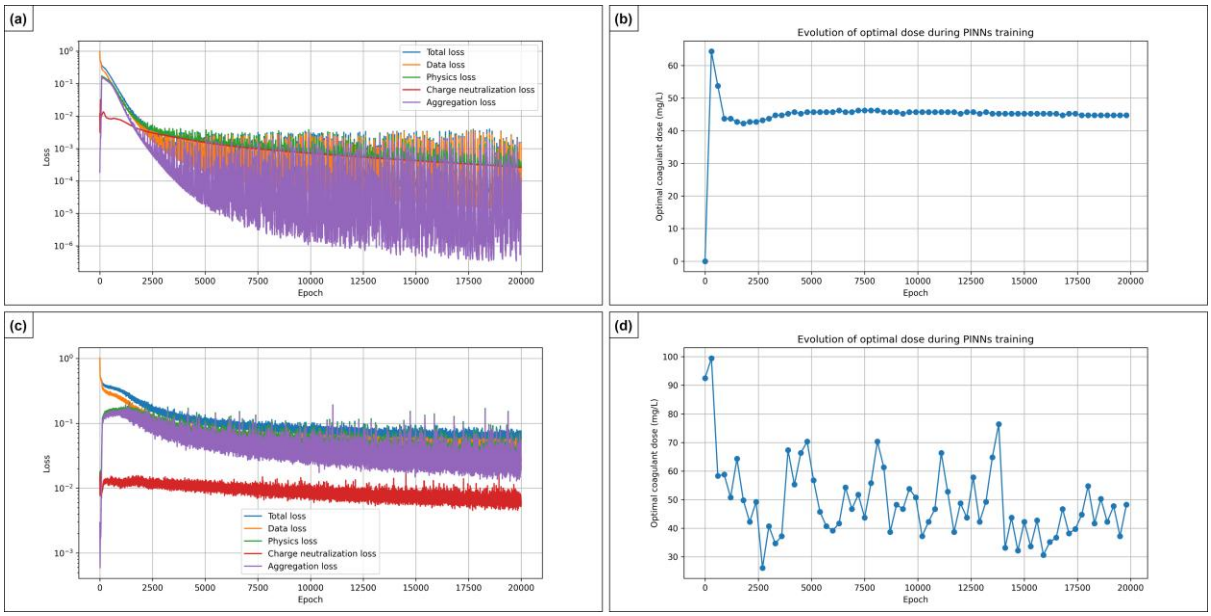



*Figure 14. Performa of invers solution to approximate coagulant optimal dosing in flocculation-coagulation process*

Fig. 15 presents a comprehensive evaluation of the proposed RTS-VG PINNs framework in approximating key physicochemical parameters, specifically turbidity (NTU) and zeta potential, in comparison with conventional machine learning models. The results highlight the advantages of incorporating physical constraints into the learning process.

The training behavior under a curriculum learning strategy is shown in Fig. 15(a), where different loss components, including data loss, zeta potential loss, and aggregation-related physics loss, are progressively minimized. The staged reduction of loss indicates stable convergence and effective balancing between data fidelity and physics-based constraints. Notably, the physics-informed components guide the model toward physically consistent solutions, avoiding overfitting to noisy observations.

The predictive relationships between coagulant dosage and process variables are illustrated in Fig. 15(b) and Fig. 15(c). For turbidity (NTU), the PINNs model captures the expected nonlinear behavior, including the initial decrease due to aggregation and the subsequent increase at higher dosages, reflecting overdosing effects. In contrast, traditional machine learning models such as Random Forest, SVM, MLP, and Gradient Boosting exhibit limited capability in capturing this complex trend, often producing oversimplified or biased predictions. Similarly, for zeta potential, the PINNs model successfully represents the nonlinear adsorption behavior, including the transition from charge neutralization to saturation, while other models fail to maintain physical consistency across the full dosage range.

The parity plots in Fig. 15(d) and Fig. 15(e) further evaluate prediction accuracy by comparing model outputs with ground truth values. The PINNs predictions show a stronger alignment along the diagonal trend, indicating better agreement with experimental observations. Although some dispersion is present, particularly in NTU predictions due to inherent process variability, the overall trend demonstrates improved predictive reliability.

A quantitative comparison using the coefficient of determination ($R^2$) is presented in Fig. 15(f). The proposed PINNs framework achieves the highest performance ($R^2 = 0.498$), outperforming Random Forest ($R^2 = 0.484$), Gradient Boosting ($R^2 = 0.434$), Support Vector Machine ($R^2 = 0.285$), and Multilayer Perceptron ($R^2 = 0.063$). This improvement highlights the benefit of embedding physical knowledge into the learning process, particularly in scenarios with limited and noisy data.

The results demonstrate that the RTS-VG PINNs framework provides more accurate and physically consistent predictions compared to purely data-driven approaches. By incorporating governing equations such as Langmuir

adsorption kinetics and aggregation–breakup dynamics, the model achieves superior generalization and interpretability, making it a robust tool for coagulant dosage optimization in flocculation–coagulation systems.

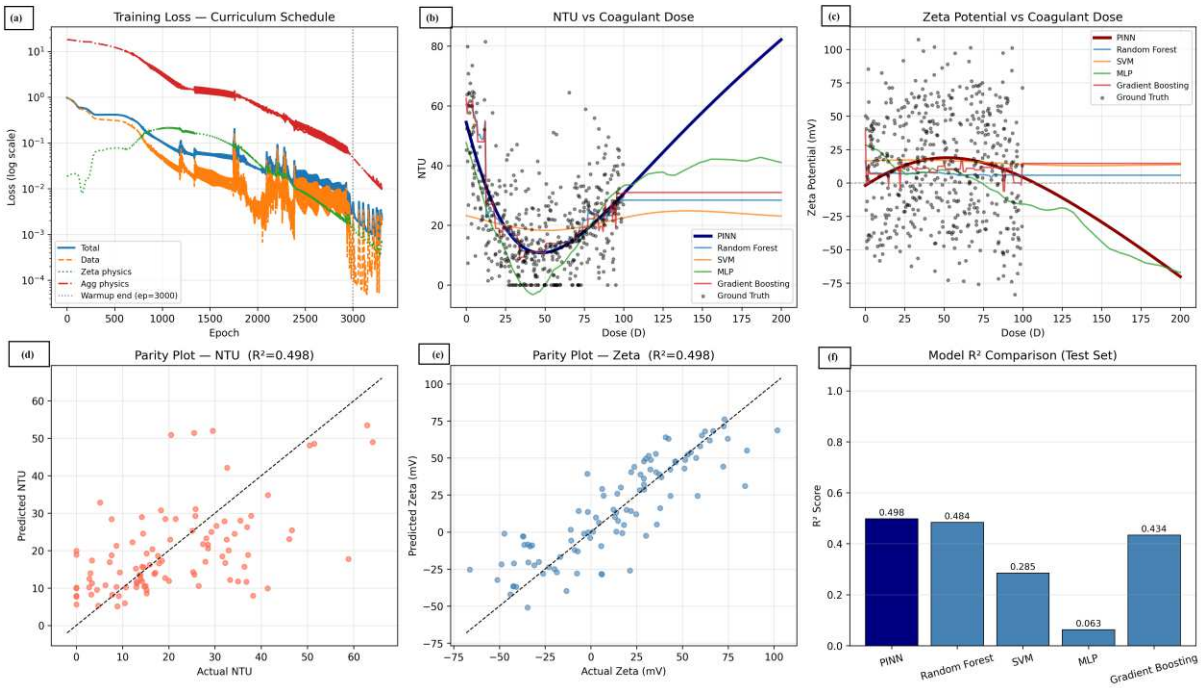



*Figure 15. Accuracy of the learning parameter approximation compared to another Machine Learning model*

## IV. LIMITATION AND FUTURE RESEARCH

This study adopts a simplified one-dimensional Kynch partial differential equation (PDE) to represent the flocculation–sedimentation process. Although the model is enhanced through the incorporation of a time-varying sedimentation velocity $v_0(t)$, real systems inherently exhibit complex three-dimensional hydrodynamics and spatial heterogeneity. Future research should therefore consider extending the current framework by integrating visual information with more advanced physical models, such as computational fluid dynamics (CFD), to better capture multidimensional flow behavior and particle interactions.

In addition, the present formulation assumes that $v_0(t)$ is the primary time-varying parameter linking visual features to physical dynamics. While this assumption provides a tractable and effective representation, it may not fully capture all visually observable phenomena associated with floc evolution. Further investigation is needed to determine whether additional time-dependent parameters, such as floc size distribution, porosity, or aggregation efficiency, should be incorporated, potentially through more flexible or higher-dimensional parameterization schemes.

The experiments conducted in this study are limited to laboratory-scale conditions. Extending the proposed RTS-VG PINNs framework to pilot-scale and full-scale industrial thickeners remains an important direction for future work. Such environments introduce additional complexities, including process variability, measurement noise, and operational disturbances, which may impact model performance. In particular, real-world conditions such as fluctuating lighting, weather variability, and electromagnetic interference from industrial equipment can degrade the quality of visual data acquisition, thereby affecting the reliability of the inferred $v_0(t)$.

Furthermore, future studies should explore the integration of mineralogical and physicochemical characterization to better understand aggregation mechanisms at the microscale. Incorporating advanced modeling approaches, such as population balance models (PBMs), could provide deeper insight into particle-level interactions, including aggregation and heteroaggregation phenomena. Such developments would enhance the interpretability and applicability of the proposed framework, supporting its deployment in more complex and realistic water treatment scenarios

## V. CONCLUSIONS

This study presents a novel real-time sensor and visual information-guided Physics-Informed Neural Network (RTS-VG PINNs) framework for modeling and optimizing flocculation–coagulation processes. By integrating multimodal data, specifically real-time turbidity measurements and image-based features, with first-principles physical models, the proposed approach addresses a fundamental limitation of conventional monitoring systems, namely the inherent time lag in turbidity-based observations. The incorporation of visual information enables early-stage detection of floc evolution, which is further translated into physically meaningful parameters such as the time-varying sedimentation velocity $v_0(t)$, thereby enhancing the predictive capability of the model.

In the direct problem, the PINNs framework successfully reconstructs the spatiotemporal distribution of floc density $\phi(t,z)$, demonstrating strong agreement with experimental observations while maintaining low PDE residuals. This highlights the model's ability to infer internal system states that are otherwise difficult to measure directly. In the inverse problem, the framework effectively estimates optimal coagulant dosage by embedding Langmuir adsorption kinetics and aggregation–breakup dynamics into the learning process. Comparative results show that the proposed method outperforms conventional machine learning models, including Random Forest, Gradient Boosting, Support Vector Machine, and Multilayer Perceptron, particularly under conditions of limited and noisy data.

The integration of visual perception with physics-informed learning not only improves prediction accuracy but also enhances interpretability and robustness. Furthermore, the incorporation of uncertainty-aware training (e.g., Monte Carlo dropout) demonstrates the model's capability to handle variability and provide more reliable predictions. Overall, the RTS-VG PINNs framework offers a powerful and flexible approach for real-time monitoring and control of flocculation–coagulation systems.

These findings suggest that combining data-driven learning with physical knowledge and visual information can significantly advance intelligent water treatment processes. The proposed framework provides a promising foundation for future development toward adaptive, real-time optimization and deployment in more complex industrial environments


## ACKNOWLEDGMENT

This research is funded by Hibah P2MI ITB (Project ID: STEI.PPMI-1-39-2026). This research was partially supported by the *Peningkatan Kualitas Publikasi Internasional Program Magister Doktor Sarjana Unggul* (PKPI-PMDSU) program, in collaboration between Institut Teknologi Bandung and the University of Groningen. The authors gratefully acknowledge Prof. Bayu Jayawardhana for his valuable contributions in the form of review and conceptual guidance.


## CRediT Authorship Contribution Statement

**Galang Adira Prayoga**: Writing – review & editing, Writing – original draft, Visualization, Software, Formal analysis, Data curation, Conceptualization. **Emir Husni**: review, Validation, Supervision, Resources, Funding acquisition. **Reza Darmakusuma**: review, Validation, Supervision, Resources. **Herto Dwi Ariesyady**: review & editing, Validation, Supervision, Resources.

## Declaration of Competing Interest

The authors declare that they have no known competing financial interests or personal relationships that could have appeared to influence the work reported in this paper.

## Data availability

Data will be made available on request.

**Consent to Publish**: Not applicable.

The authors confirm that this manuscript has not been published elsewhere and is not under consideration by another journal. All authors have reviewed and approved the final version of the manuscript for publication.

**Consent to Participate**: Not applicable.

This study did not involve human participants or animals; therefore, consent to participate was not required.

**Ethics Approval**: Not applicable.

This study did not involve human participants, animals, or clinical data. Therefore, ethical approval was not required.

**REFERENCES**


[1] P. Jarvis, B. Jefferson, J. Gregory, dan S. A. Parsons, "A review of floc strength and breakage," *Water Res.*, vol. 39, no. 14, hal. 3121–3137, 2005, doi: https://doi.org/10.1016/j.watres.2005.05.022.

[2] G. El Mouhri *dkk.*, "Evaluating the effectiveness of coagulation–flocculation treatment on a wastewater from the moroccan leather tanning industry : An ecological approach," *Heliyon*, vol. 10, no. 5, hal. e27056, 2024, doi: 10.1016/j.heliyon.2024.e27056.

[3] C. C. Davis, M. Edwards, W. R. Knocke, J. C. Little, dan P. J. Vikesland, "Understanding and Predicting Water Quality Impacts on Coagulation," 2014.

[4] L. Ge *dkk.*, "Research Progress in Flocculation Treatment of Aggregate Washing Wastewater : Mechanisms , Innovations , and Challenges," *Separations*, vol. 13, hal. 1–21, 2026.

[5] L. Zhang, X. Liu, M. Zhang, T. Wang, dan H. Tang, "The effect of pH / PAC on the coagulation of anionic surfactant wastewater generated in the cosmetic production," *J. Environ. Chem. Eng.*, vol. 11, no. 2, hal. 109312, 2023, doi: 10.1016/j.jece.2023.109312.

[6] P. Filip dan M. Pivokonsky, "The Impact of Low Temperature on the Efficiency of Coagulation / Flocculation Process in Drinking Water Treatment," *Environments*, vol. 13, no. 40, 2026.

[7] A. Mortadi *dkk.*, "Complex electrical conductivity as a new technique to monitor the coagulation-flocculation processes in the wastewater treatment of the textile Industry," *Water Resour. Ind.*, vol. 24, hal. 100130, 2020, doi: 10.1016/j.wri.2020.100130.

[8] M. Getahun, A. Befekadu, dan E. Alemayehu, "Coagulation process for the removal of color and turbidity from wet coffee processing industry wastewater using bio-coagulant : Optimization through central composite design," *Heliyon*, vol. 10, no. 7, hal. e27584, 2024, doi: 10.1016/j.heliyon.2024.e27584.

[9] Y. S. Vadasarukkai dan G. A. Gagnon, "Influence of the Mixing Energy Consumption A ff ecting Coagulation and Floc Aggregation," *Environ. Sci. Technol.*, vol. 51, hal. 3480–3489, 2017, doi: 10.1021/acs.est.6b06281.

[10] A. Rosińska dan L. Dąbrowska, "Influence of type and dose of coagulants on effectiveness of PAH removal in coagulation water treatment," *Water Sci. Eng.*, vol. 14, no. 3, hal. 193–200, 2021, doi: https://doi.org/10.1016/j.wse.2021.08.004.

[11] F. Nyström, K. Nordqvist, I. Herrmann, A. Hedström, dan M. Viklander, "Laboratory scale evaluation of coagulants for treatment of stormwater," *J. Water Process Eng.*, vol. 36, hal. 101271, 2020, doi: https://doi.org/10.1016/j.jwpe.2020.101271.

[12] M. Kroupa, M. Vonka, dan J. Kosek, "Modeling the Mechanism of Coagulum Formation in Dispersions," *Langmuir*, hal. 2693–2702, 2014.

[13] M. Kalhormohammadi dan S. Khoramipour, "Predictive modeling of coagulant dosing in drilling wastewater treatment using artificial neural networks," *Sci. Rep.*, vol. 15, hal. 1–16, 2025.

[14] E. Song dan S. K. Han, "Real-Time Sensor-Controlled Coagulant Dosing and Pressure in a Novel Sludge Dewatering System," *Clean Technol.*, vol. 7, hal. 1–21, 2025.

[15] S. Li, Y. Liu, Z. Wang, C. Dou, W. Zhao, dan H. Shu, "Constructing a visual detection method for coagulation effect based on image feature machine learning," *J. Water Process Eng.*, vol. 68, hal. 106354, 2024, doi: https://doi.org/10.1016/j.jwpe.2024.106354.

[16] M. S. Nasser dan A. E. James, "Degree of flocculation and viscoelastic behaviour of kaolinite-sodium chloride dispersions," *Colloids Surfaces A Physicochem. Eng. Asp.*, vol. 315, no. 1, hal. 165–175, 2008, doi: https://doi.org/10.1016/j.colsurfa.2007.07.030.

[17] S. Du, Y. Chang, Y. Wang, dan H. Wang, "Visual Information-guided Physics-Informed Neural Network ( VI-PINN ) for predictive forecasting and control of the flocculation sedimentation process," *Miner. Eng.*, vol. 232, no. June, hal. 109504, 2025, doi: 10.1016/j.mineng.2025.109504.

[18] A. Rymszewicz *dkk.*, "Measurement differences between turbidity instruments , and their implications for suspended sediment concentration and load calculations : A sensor inter-comparison study," *J.*

*Environ. Manage.*, vol. 199, hal. 99–108, 2017, doi: 10.1016/j.jenvman.2017.05.017.

[19] L. Wang, D. Wang, A. James, S. Cuthbertson, dan Q. Chen, "Experimental measurement of flocculation and settling behavior in fine sediments from the Three Gorges Reservoir , China," *Int. J. Sediment Res.*, vol. 40, no. 6, hal. 954–971, 2025, doi: 10.1016/j.ijsrc.2025.07.001.

[20] W. Wu, Y. Wang, H. Zhang, M. Zhang, dan M. Chiu, "Phased Long Short-Term Memory-Based Predictive Control of Chemical Processes With Asynchronous and Delayed Measurements," *IEEE Trans. Control Syst. Technol.*, vol. 33, no. 6, hal. 2439–2454, 2025, doi: 10.1109/TCST.2025.3587908.

[21] G. E. Karniadakis, I. G. Kevrekidis, L. Lu, P. Perdikaris, S. Wang, dan L. Yang, "Physics-informed machine learning," *Nat. Rev. Phys.*, vol. 3, no. 6, hal. 422–440, 2021, doi: 10.1038/s42254-021-00314-5.

[22] C. Matovelle dan D. Heras, "Machine Learning Techniques in Dosing Coagulants and Biopolymers for Treating Leachate Generated in Landfills," *Water*, no. 15, hal. 4200, 2023.

[23] A. Moussouni *dkk.*, "Ensemble learning-driven optimization of coagulant dosing for drinking water treatment plants using a scalable framework for smart and sustainable process control," *Environ. Res.*, vol. 288, no. P1, hal. 123229, 2026, doi: 10.1016/j.envres.2025.123229.

[24] H. Tahraoui, A. Belhadj, dan N. Moula, "Optimisation and Prediction of the Coagulant Dose for the Elimination of Organic Micropollutants Based on Turbidity," *J. Chem. Chem. Eng. Croat.*, vol. 70, hal. 675–691, 2021.

[25] J. Chauhan, R. M. Rani, V. Prashanthi, H. Almujibah, A. Alshahri, dan K. Srinivas, "Gradient-Boosted Decision Tree with used Slime Mould Algorithm (SMA) for wastewater treatment systems," *Water Reuse*, vol. 13, no. 3, hal. 393–410, 2023, doi: 10.2166/wrd.2023.046.

[26] S. Xu, S. Wang, Y. Yang, L. Zheng, dan F. Xiao, "Importance analysis of key parameters for coagulation dosage prediction based on machine learning models," *Process Saf. Environ. Prot.*, vol. 205, no. August 2025, hal. 108152, 2026, doi: 10.1016/j.psep.2025.108152.

[27] X. Chen, W. Li, T. Xia, dan R. Ouyang, "Data-Driven Methods and Artificial Intelligence in Reliability and Maintenance : A Review," *Mathematics*, vol. 14, no. 899, hal. 1–49, 2026.

[28] C. Yang, Y. Zhang, M. Huang, dan H. Liu, "Adaptive dynamic prediction of effluent quality in wastewater treatment processes using partial least squares embedded with relevance vector machine," *J. Clean. Prod.*, vol. 314, no. June, hal. 128076, 2021, doi: 10.1016/j.jclepro.2021.128076.

[29] M. Raissi, P. Perdikaris, dan G. E. Karniadakis, "Physics-informed neural networks: A deep learning framework for solving forward and inverse problems involving nonlinear partial differential equations," *J. Comput. Phys.*, vol. 378, hal. 686–707, 2019, doi: 10.1016/j.jcp.2018.10.045.

[30] B. E. Mokhtari, C. Chauviere, dan P. Bonnet, "On the Importance of the Mathematical Formulation to Get PINNs Working," *IEEE Trans. Electromagn. Compat.*, vol. 66, no. 6, hal. 2142–2149, 2024, doi: 10.1109/TEMC.2024.3490699.

[31] B. C. Geiger dan S. Member, "Data vs . Physics : The Apparent Pareto Front of Physics-Informed Neural Networks," *IEEE Access*, vol. 11, no. July, 2023, doi: 10.1109/ACCESS.2023.3302892.

[32] B. Y. G. J. Kynch, "A theory of sedimentation," *Univ. Birmingham*, 1951.

[33] K. L. Wu dan S. K. Lai, "Theoretical Studies of the Early Stage Coagulation Kinetics for a Charged Colloidal Dispersion," *Langmuir*, vol. 21, no. 8, hal. 3238–3246, Apr 2005, doi: 10.1021/la0476682.

[34] Y. Liu dan L. Shen, "From Langmuir Kinetics to First- and Second-Order Rate Equations for Adsorption," *Langmuir*, vol. 24, no. 20, hal. 11625–11630, Okt 2008, doi: 10.1021/la801839b.

[35] G. Chen, C. Li, Z. Ruan, R. Bürger, dan H. Hou, "Research on floc structure and physical properties based on pipeline flocculation," *J. Water Process Eng.*, vol. 53, no. November 2022, hal. 103627, 2023, doi: 10.1016/j.jwpe.2023.103627.

[36] H. Yamamura, E. U. Putri, T. Kawakami, A. Suzuki, H. D. Ariesyady, dan T. Ishii, "Dosage optimization of polyaluminum chloride by the application of convolutional neural network to the floc images captured in jar tests," *Sep. Purif. Technol.*, vol. 237, no. October 2019, hal. 116467, 2020, doi:

10.1016/j.seppur.2019.116467.

[37] B. Gao, Y. Chu, Q. Yue, B. Wang, dan S. Wang, “Characterization and coagulation of a polyaluminum chloride ( PAC ) coagulant with high Al 13 content,” *J. Environ. Manage.*, vol. 76, hal. 143–147, 2005, doi: 10.1016/j.jenvman.2004.12.006.

[38] K. He dan J. Sun, “Deep Residual Learning for Image Recognition,” *Comput. Vis. Found.*, hal. 1–9, 2015.

[39] M. Hussain, “YOLO-v1 to YOLO-v8 , the Rise of YOLO and Its Complementary Nature toward Digital Manufacturing and Industrial Defect Detection,” *Machines*, vol. 11, 2023.

[40] R. Sapkota dan M. Karkee, “Ultralytics YOLO Evolution: An Overview of YOLO26, YOLO11, YOLOv8 and YOLOv5 Object Detectors for Computer Vision and Pattern Recognition,” *arXiv*, vol. 26, hal. 1–16, 2025.

[41] G. A. Prayoga dan E. Husni, “An Inverse Problem of Determining the Parameters in Multiphysics Problem by Using Fractional Physics-Informed Neural Networks,” *Int. J. Electr. Eng. Informatics*, vol. 17, no. 4, hal. 588–611, 2025, doi: 10.15676/ijeei.2025.17.4.1.